

## Article

# Adaptive Non-Singular Fast Terminal Sliding Mode Trajectory Tracking Control for Robot Manipulators

Qiyao Yang <sup>1,2</sup> , Xiangfeng Ma <sup>3</sup>, Wei Wang <sup>3</sup> and Dongliang Peng <sup>1,\*</sup>

<sup>1</sup> School of Automation, Hangzhou Dianzi University, Xiasha Higher Education Zone, Hangzhou 310018, China

<sup>2</sup> College of Electrical Engineering, Zhejiang University of Water Resources and Electric Power, Hangzhou 310018, China

<sup>3</sup> CSSC System Engineering Research Institute, Beijing 100094, China

\* Correspondence: dlpeng@hdu.edu.cn; Tel.: +86-0571-86873828

**Abstract:** In order to improve the efficiency of human–robot interaction (HRI), it is necessary to carry out research on precise control of the manipulator. In this paper, an adaptive non-singular fast terminal sliding mode control scheme is proposed for robot manipulators to solve the trajectory tracking problem with model uncertainty and external disturbances. At first, a novel non-singular fast terminal sliding mode surface is proposed, and by introducing an auxiliary function, the singularity problem caused by the inverse of the error-related matrix could be avoided in the controller design process. Then, the controller is developed by using Lyapunov synthesis. A robust adaptive strategy is used to deal with lumped uncertainty, with an adaptive update law designed to compensate for the upper bound of lumped uncertainty whose upper bound is prior unknown. Finally, a two-link robot manipulators as a simulation example is given to illustrate the effectiveness of the proposed scheme. Compared with other similar algorithms, the proposed adaptive non-singular fast terminal sliding mode control scheme has higher efficiency and smaller computational complexity for the reason that no piecewise continuous function is needed to be constructed during the controller design.



**Citation:** Yang, Q.; Ma, X.; Wang, W.; Peng, D. Adaptive Non-Singular Fast Terminal Sliding Mode Trajectory Tracking Control for Robot Manipulators. *Electronics* **2022**, *11*, 3672. <https://doi.org/10.3390/electronics11223672>

Academic Editor: Ahmed Al-Durra

Received: 12 October 2022

Accepted: 7 November 2022

Published: 10 November 2022

**Publisher's Note:** MDPI stays neutral with regard to jurisdictional claims in published maps and institutional affiliations.



**Copyright:** © 2022 by the authors. Licensee MDPI, Basel, Switzerland. This article is an open access article distributed under the terms and conditions of the Creative Commons Attribution (CC BY) license (<https://creativecommons.org/licenses/by/4.0/>).

**Keywords:** robot manipulators; non-singular fast terminal sliding mode; adaptive control; finite-time convergence

## 1. Introduction

Robot manipulators play an important role in human–robot interaction (HRI). So far, they have been widely applied in the manufacturing industry, medical treatment, cargo handling, space exploration and so on to improve automation and efficiency. In the dynamics of robot manipulators, there exist complicated inherent characteristics, such as load variation, hysteresis, friction and coupling, which make the control issues challenging and nontrivial. In order to achieve the accurate control objective of positioning tracking, some feedback control strategies have been proposed in the past decades, such as decentralized control [1], feedback linearization [2], PID control [3], iterative learning control [4],  $H_\infty$  control [5], robust control [6], neural network control [7] and sliding mode control (SMC) [8].

SMC has many advantages, e.g., fast response and strong robustness to the variety of system parameters and external disturbances. Additionally, SMC is convenient in physical implementation for free of online system identification. Based on the above merits, SMC algorithms for robot manipulator have been reported in many works in the literature [8–12]. Specifically, Zhang et al. investigated the trajectory tracking control based on smooth second-order sliding mode for robot manipulators [8]. Zhao et al. studied the sliding mode control for a two-joint coupling nonlinear system based on extended state observer [9]. In [10], Baek et al. presented a new adaptive SMC scheme that uses the time-delay estimation technique and applied the scheme to robot manipulators. In [11], Van et al. developed an adaptive fuzzy fault tolerant SMC strategy for robot manipulators. In [12], Tran et al.

investigated the backstepping adaptive sliding mode control for an electrohydraulic elastic manipulator in the presence of the matched and unmatched uncertainties. The SMC algorithms given in literature [8–12] can ensure that the tracking error asymptotically converges to zero or its neighborhood.

Unlike these traditional SMC schemes, terminal SMC aims at converging to zero within a finite time, which motivates people to research and develop terminal SMC schemes for practical applications [13]. The potential singularity is an obstacle for applying terminal SMC theoretical algorithms into industrial applications because the singularity means that the value of the control input is infinite. In order to overcome the singularity problem, some nonsingular terminal SMC strategies have been proposed in the literature [14–17]. In [14], a robust nonsingular terminal SMC method was proposed for rigid manipulator systems with unmodeled dynamics and external disturbances. The further investigation of [14] was reported in [15], where a novel terminal SMC approach was developed to improve the convergence speed and tracking accuracy. In [16], an integral nonsingular terminal sliding mode surface was constructed for the SMC design of manipulators with unmodeled dynamics and unknown external disturbances. In [17], a second-order fast nonsingular terminal SMC approach was proposed for robotic systems with external disturbances and inertial uncertainties, which can make the tracking error quickly converge to zero, with the chattering phenomena of control signal avoided. So far, the most popular strategy to deal with singularity problems is to construct piecewise continuous sliding mode surfaces [14–17]. However, this solution have two flaws. First, it is not an easy job to construct a piecewise continuous sliding mode surface. Second, the online computation load is very large while such a control system runs.

Based on the above analysis, we obtain the following consequent conclusions: (1) It is worthwhile to investigate the terminal SMC scheme free of constructing piecewise continuous sliding mode surface. (2) It is necessary to study how to lighten the online calculation burden of closed-loop systems and reduce the analysis difficulty of finite-time stability during controller design.

In this paper, an adaptive nonsingular fast terminal SMC (ANSFTSMC) approach is proposed for a class of robot manipulators with internal uncertainties and external disturbances such that the tracking error can converge to the neighborhood of the origin during a finite time. The main contributions are as follows. First, a new terminal sliding surface is designed to avoid the occurrence of singularity problem. Second, during control law design, an auxiliary function method is developed to overcome the singular problem caused by matrix inversion. Compared with the traditional piecewise continuous function methods, the auxiliary function method can reduce the design difficulty and the burden computation. Third, robust adaptive method is used to design feedback term to compensate for the sum of uncertainties, whose upper bound need not be prior known.

The remainder of this paper is organized as follows. The problem formulation is presented in Section 2. The construction of a nonsingular fast terminal sliding mode surface, the detailed design process of controller and stability analysis are introduced in Section 3. The simulation results are shown in Section 4. Finally, Section 5 concludes this work.

## 2. Problem Formulation

Consider an  $n$  degrees-of-freedom rigid manipulator, whose dynamic equation is expressed by [17]

$$M(\mathbf{q})\ddot{\mathbf{q}} + C(\mathbf{q}, \dot{\mathbf{q}})\dot{\mathbf{q}} + \mathbf{G}(\mathbf{q}) = \boldsymbol{\tau} + \mathbf{d} \quad (1)$$

where  $\mathbf{q} = [q_1, q_2, \dots, q_n]^T \in \mathbb{R}^n$  is the vector of joint angular position,  $M(\mathbf{q}) \in \mathbb{R}^{n \times n}$  is a symmetric positive definite inertia matrix,  $C(\mathbf{q}, \dot{\mathbf{q}}) \in \mathbb{R}^n$  represents the vector of centripetal and Coriolis torques,  $\mathbf{G}(\mathbf{q}) \in \mathbb{R}^n$  is the gravitational force,  $\boldsymbol{\tau} \in \mathbb{R}^n$  is the input torque, and  $\mathbf{d} = [d_1, d_2, \dots, d_n]^T \in \mathbb{R}^n$  represents the sum of external disturbances and unmodeled dynamics.

Due to modeling errors, physical parameter perturbations and other factors, there exist some unmodeled dynamics in robot manipulator systems as follows:

$$\begin{cases} M(\mathbf{q}) = M_0(\mathbf{q}) + \Delta M(\mathbf{q}) \\ C(\mathbf{q}, \dot{\mathbf{q}}) = C_0(\mathbf{q}, \dot{\mathbf{q}}) + \Delta C(\mathbf{q}, \dot{\mathbf{q}}) \\ \mathbf{G}(\mathbf{q}) = \mathbf{G}_0(\mathbf{q}) + \Delta \mathbf{G}(\mathbf{q}) \end{cases} \quad (2)$$

where  $M_0(\mathbf{q})$ ,  $C_0(\mathbf{q}, \dot{\mathbf{q}})$  and  $\mathbf{G}_0(\mathbf{q})$  are the nominal components of robot manipulator systems;  $\Delta M(\mathbf{q})$ ,  $\Delta C(\mathbf{q}, \dot{\mathbf{q}})$ ,  $\Delta \mathbf{G}(\mathbf{q})$  are uncertainties.

Combining (2) with (1) leads to

$$M_0(\mathbf{q})\ddot{\mathbf{q}} + C_0(\mathbf{q}, \dot{\mathbf{q}})\dot{\mathbf{q}} + \mathbf{G}_0(\mathbf{q}) = \boldsymbol{\tau} + \mathbf{d}_\Sigma \quad (3)$$

where  $\mathbf{d}_\Sigma = \mathbf{d} - \Delta M(\mathbf{q})\ddot{\mathbf{q}} - \Delta C(\mathbf{q}, \dot{\mathbf{q}})\dot{\mathbf{q}} - \Delta \mathbf{G}(\mathbf{q})$ . Let  $\mathbf{x}_1 = \mathbf{q}, \mathbf{x}_2 = \dot{\mathbf{q}}$ . Then, (3) may be rewritten as

$$\begin{cases} \dot{\mathbf{x}}_1 = \mathbf{x}_2 \\ \dot{\mathbf{x}}_2 = M_0^{-1}(\mathbf{x}_1) [\mathbf{d}_\Sigma + \boldsymbol{\tau} - C_0(\mathbf{x}_1, \mathbf{x}_2)\mathbf{x}_2 - \mathbf{G}_0(\mathbf{x}_1)] \end{cases} \quad (4)$$

Let us define  $\mathbf{e}_1$  and  $\mathbf{e}_2$  as follows:

$$\begin{cases} \mathbf{e}_1 = [e_{11}, e_{12}, \dots, e_{1n}]^T = \mathbf{x}_1 - \mathbf{x}_d \\ \mathbf{e}_2 = [e_{21}, e_{22}, \dots, e_{2n}]^T = \dot{\mathbf{x}}_1 - \dot{\mathbf{x}}_d \end{cases} \quad (5)$$

where  $\mathbf{x}_d = \mathbf{q}_d = [q_{1d}, q_{2d}, \dots, q_{nd}]^T$  is the reference trajectory. From (4) and (5), we can obtain the error dynamic equation as

$$\begin{cases} \dot{\mathbf{e}}_1 = \mathbf{e}_2 \\ \dot{\mathbf{e}}_2 = \mathbf{F} + \mathbf{D} + M_0^{-1}(\mathbf{x}_1)\boldsymbol{\tau} \end{cases} \quad (6)$$

where  $\mathbf{F} = -M_0^{-1}(\mathbf{x}_1)(C_0(\mathbf{x}_1, \mathbf{x}_2)\mathbf{x}_2 + \mathbf{G}_0(\mathbf{x}_1)) - \dot{\mathbf{x}}_d$ ,  $\mathbf{D} = M_0^{-1}(\mathbf{x}_1)\mathbf{d}_\Sigma$ .

Based on the above system descriptions, the following lemmas and assumptions are given in this article.

**Lemma 1 ([18]).** For a given system  $\dot{x} = f(x)$ , if there exists a continuous non-negative function  $V(x)$  and scalars  $\alpha > 0, \beta > 0, 0 < \gamma < 1$  and  $0 < \eta < +\infty$  such that  $\dot{V}(x) \leq -\alpha V - \beta V^\gamma + \eta$  holds, then the system  $\dot{x} = f(x)$  is finite-time stable, that is,  $x$  converges to a small residual set

$$\left\{ \lim_{t \rightarrow T} x \mid V(x) \leq \min \left\{ \left( \frac{\eta}{(1-\mu)\alpha} \right), \left( \frac{\eta}{(1-\mu)\beta} \right)^{\frac{1}{\gamma}} \right\} \right\} \text{ in a finite time, where } 0 < \mu < 1,$$

$$T \leq \max \left\{ t_0 + \frac{1}{\mu\alpha(1-\gamma)} \ln \frac{\mu\alpha V^{1-\gamma}(t_0) + \beta}{\beta}, t_0 + \frac{1}{\alpha(1-\gamma)} \ln \frac{\mu\alpha V^{1-\gamma}(t_0) + \mu\beta}{\mu\beta} \right\}. \quad (7)$$

Here,  $t_0$  indicates the initial time of control system operation.

**Lemma 2 ([19]).** For  $\phi \in \mathbb{R}, \varphi \in \mathbb{R}$ , and any constants  $p > 0, q > 0, m > 0$ , the following inequality holds:

$$|\phi|^p |\varphi|^q \leq \frac{p}{p+q} m |\phi|^{p+q} + \frac{q}{p+q} m^{-\frac{p}{q}} |\varphi|^{p+q} \quad (8)$$

**Lemma 3** ([20]). For any positive number  $x_i, i = 1, 2, \dots, n$ , there exists a constant  $r$ , which satisfies

$$\sum_{i=1}^n x_i^r \geq \left( \sum_{i=1}^n x_i \right)^r, \quad 0 < r < 1. \tag{9}$$

**Assumption 1** ([14]). The sum of uncertainties  $\mathbf{D}$  meets the following inequality:

$$\|\mathbf{D}\| \leq b_1 + b_2\|\mathbf{x}_1\| + b_3\|\dot{\mathbf{x}}_1\|^2 = \mathbf{b}^T \Phi, \tag{10}$$

where  $\mathbf{b} = [b_1, b_2, b_3]^T, \Phi = [1, \|\mathbf{x}_1\|, \|\dot{\mathbf{x}}_1\|]^T$ . Here,  $b_i$  is a positive constant for  $i = 1, 2, 3$ ; the operator  $\|\cdot\|$  means taking the Euclidean norm for  $\cdot$ .

The control objective of this paper is to design an adaptive nonsingular fast terminal sliding mode controller  $\tau$  for the system (4) to make the joint position of the manipulator  $\mathbf{x}_1$  track the reference trajectory  $\mathbf{x}_d$  in a finite time. In addition, by constructing a nonsingular terminal sliding surface and auxiliary function, the singularity problem is avoided during the controller design.

### 3. Main Results

#### 3.1. Design of Nonsingular Fast Terminal Sliding Surface and Control Law

On the basis of (6), we construct a novel nonsingular fast terminal sliding surface as

$$S_i = e_{1i} + \frac{k_2 a}{2a - 1} \cdot \text{sig}^{2-\frac{1}{a}}(e_{2i} + k_1 e_{1i}), i = 1, \dots, n \tag{11}$$

where  $k_1 > 0, k_2 > 0, a > 1$  and  $\text{sig}^{2-\frac{1}{a}}(e_{2i} + k_1 e_{1i}) = |e_{2i} + k_1 e_{1i}|^{2-\frac{1}{a}} \text{sgn}(e_{2i} + k_1 e_{1i})$ , with  $\text{sgn}(\cdot)$  being a symbolic function operator.

When  $S_i = 0$ , it follows from (11) that

$$\dot{e}_{1i} = -k_1 e_{1i} - \bar{k}_2 \text{sig}^{\bar{a}} e_{1i}, \tag{12}$$

where  $\bar{k}_2 = \left( \frac{2a-1}{k_2 a} \right)^{\frac{a}{2a-1}}, \bar{a} = \frac{a}{2a-1}$ . Let us define

$$V_1 = \frac{1}{2} \sum_{i=1}^n e_{1i}^2. \tag{13}$$

Taking the derivative of  $V_1$  with respect to time yields

$$\begin{aligned} \dot{V}_1 &= \sum_{i=1}^n e_{1i} \dot{e}_{1i} \\ &= -\bar{k}_1 \sum_{i=1}^n e_{1i}^2 - \bar{k}_2 \sum_{i=1}^n |e_{1i}|^{1+\bar{a}} \\ &\leq -2\bar{k}_1 V_1 - \bar{k}_2 2^{\frac{1+\bar{a}}{2}} V_1^{\frac{1+\bar{a}}{2}}, \end{aligned} \tag{14}$$

where  $0 < \frac{1+\bar{a}}{2} < 1$ . By Lemma 1, it follows from (13) that the tracking error  $e_{1i}$  can converge to 0 within a finite time  $T_1$ .

Let  $\mathbf{S} = [S_1, \dots, S_n]^T$ . Differentiating  $\mathbf{S}$  leads to

$$\dot{\mathbf{S}} = \mathbf{e}_2 + h(\dot{\mathbf{e}}_2 + k_1 \dot{\mathbf{e}}_1). \tag{15}$$

where  $h = \text{diag}(h_1, \dots, h_n), h_i = k_2 |e_{2i} + k_1 e_{1i}|^{1-\frac{1}{a}} \geq 0, i = 1, 2, \dots, n$ . Define an auxiliary variable  $\Psi = [\Psi_1, \dots, \Psi_n]^T$ . For  $i = 1, 2, \dots, n$ ,

$$\Psi_i = \frac{1}{k_2} \text{sig}^{\frac{1}{a}}(e_{2i} + k_1 e_{1i}) + \frac{k_1 a}{2a - 1} (e_{2i} + k_1 e_{1i}). \tag{16}$$

According to (11) and the definition of  $h$  and  $\Psi$ , we can deduce that

$$h\Psi = \mathbf{e}_2 + k_1 \mathbf{S}. \tag{17}$$

It follows from (15) and (17) that

$$\begin{aligned} \dot{\mathbf{S}} &= h(\mathbf{F} + \mathbf{D} + M_0^{-1}(\mathbf{x}_1)\boldsymbol{\tau} + k_1 \mathbf{e}_2) \\ &= h(\mathbf{F} + \mathbf{D} + \Psi + M_0^{-1}(\mathbf{x}_1)\boldsymbol{\tau} + k_1 \mathbf{e}_2) - k_1 \mathbf{S} \\ &= h(\mathbf{F} + \Psi + k_1 \mathbf{e}_2 + \mathbf{D} + M_0^{-1}(\mathbf{x}_1)\boldsymbol{\tau}) - k_1 \mathbf{S} \end{aligned} \tag{18}$$

**Remark 1.** The singularity problem may happen while the following traditional sliding mode surface (19) is used:

$$S_i = \dot{e}_{1i} + \alpha_1 e_{1i} + \alpha_2 \text{sig}^{\beta} e_{1i}, \alpha_1 > 0, \alpha_2 > 0, 0 < \beta < 1. \tag{19}$$

Differentiating (11) leads to

$$\dot{S}_i = \dot{e}_{1i} + k_2 |e_{2i} + k_1 e_{1i}|^{1-\frac{1}{a}} (\dot{e}_{2i} + k_1 \dot{e}_{1i}), \tag{20}$$

in which  $0 < 1 - \frac{1}{a} < 1$  holds such that the singularity problem can be directly avoided by constructing the novel sliding mode surface (11).

**Remark 2.** If adopting the solution given in (21), then the singularity problem happens for performing matrix inversion  $h^{-1} \mathbf{e}_2$ . We adopt an auxiliary function method (18) to solve this problem, rather than the traditional piecewise continuous function construction method. Compared to the traditional piecewise continuous function method, the computational complexity and finite-time stability analysis difficulty of the auxiliary function method can be reduced.

$$\begin{aligned} \dot{\mathbf{S}} &= \mathbf{e}_2 + h(\mathbf{F} + \mathbf{D} + M_0^{-1}(\mathbf{x}_1)\boldsymbol{\tau} + k_1 \mathbf{e}_2) \\ &= h(\mathbf{F} + h^{-1} \mathbf{e}_2 + \mathbf{D} + M_0^{-1}(\mathbf{x}_1)\boldsymbol{\tau} + k_1 \mathbf{e}_2). \end{aligned} \tag{21}$$

Based on (18), we define the nonsingular fast terminal SMC law as

$$\boldsymbol{\tau} = -M_0 [\mathbf{F}^* + \lambda_1 \mathbf{S} + \lambda_2 \text{sig}^{\gamma} \mathbf{S} + \hat{\mathbf{b}}^T \Phi \text{sgn}(\mathbf{S}^T h)] \tag{22}$$

and the adaptive law as

$$\dot{\hat{\mathbf{b}}} = \eta (||\bar{\mathbf{S}}|| \Phi - m \hat{\mathbf{b}}), \tag{23}$$

where  $\mathbf{F}^* = [F_1^*, \dots, F_n^*]^T = \mathbf{F} + \Psi + k_1 \mathbf{e}_2$ ,  $\text{sig}^{\gamma} \mathbf{S} = [\text{sig}^{\gamma} S_1, \dots, \text{sig}^{\gamma} S_n]^T$ ,  $\text{sgn}(\mathbf{S}^T h) = [\text{sgn}(S_1 h_1), \dots, \text{sgn}(S_n h_n)]^T$ ,

$\bar{\mathbf{S}} = (\mathbf{S}^T h)^T = h \mathbf{S}$ ,  $\lambda_1 > 0, \lambda_2 > 0, 0 < \gamma < 1, \eta > 0, m > 0, \hat{b}_i(0) > 0, i = 1, 2, 3$ . The control diagram of the designed SMC scheme is shown in Figure 1.

### 3.2. Stability Analysis

The finite-time stability of the robot manipulator (6) in both the reaching phase and the sliding phase is established by the following theorem.

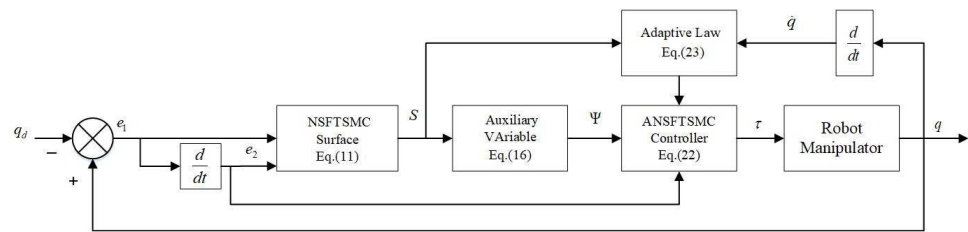


Figure 1. Control diagram of the designed SMC scheme.

**Theorem 1.** Consider the robot manipulator (6) with nonsingular sliding mode surface (11), auxiliary variable (14), finite-time controller (22) and update law (23). The system tracking error can converge to the neighborhood of the origin in finite time.

**Proof of Theorem 1.** Let us define a Lyapunov function as

$$V_2 = \frac{1}{2} \mathbf{S}^T \mathbf{S} + \frac{1}{2\eta} \tilde{\mathbf{b}}^T \tilde{\mathbf{b}}, \tag{24}$$

where  $\tilde{\mathbf{b}} = \mathbf{b} - \hat{\mathbf{b}}$ . Differentiating (24) leads to

$$\dot{V}_2 = \mathbf{S}^T \dot{\mathbf{S}} - \frac{1}{\eta} \tilde{\mathbf{b}}^T \dot{\tilde{\mathbf{b}}}. \tag{25}$$

Substituting (18) and (22) into (24) yields

$$\begin{aligned} \dot{V}_2 &= \mathbf{S}^T h(\mathbf{F}^* + \mathbf{D} + \mathbf{M}_0^{-1} \boldsymbol{\tau}) - k_1 \sum_{i=1}^n S_i^2 - \frac{1}{\eta} \tilde{\mathbf{b}}^T \dot{\tilde{\mathbf{b}}} \\ &= \mathbf{S}^T h[-\lambda_1 \mathbf{S} - \lambda_2 \text{sig}^\gamma \mathbf{S} - \tilde{\mathbf{b}}^T \boldsymbol{\Phi} \text{sgn}(\mathbf{S}^T h) + \mathbf{D}] \\ &\quad - k_1 \sum_{i=1}^n S_i^2 - \frac{1}{\eta} \tilde{\mathbf{b}}^T \dot{\tilde{\mathbf{b}}} \\ &\leq -k_1 \sum_{i=1}^n S_i^2 - \lambda_2 \sum_{i=1}^n h_i |S_i|^{1+\gamma} + \|\tilde{\mathbf{S}}\| \tilde{\mathbf{b}}^T \boldsymbol{\Phi} - \frac{1}{\eta} \tilde{\mathbf{b}}^T \dot{\tilde{\mathbf{b}}} \\ &= -k_1 \sum_{i=1}^n S_i^2 - \lambda_2 \sum_{i=1}^n h_i |S_i|^{1+\gamma} + \tilde{\mathbf{b}}^T (\|\tilde{\mathbf{S}}\| \boldsymbol{\Phi} - \frac{1}{\eta} \dot{\tilde{\mathbf{b}}}) \end{aligned} \tag{26}$$

Substituting (23) into (26), we have

$$\dot{V}_2 = -k_1 \sum_{i=1}^n S_i^2 - \lambda_2 \sum_{i=1}^n h_i |S_i|^{1+\gamma} + m \tilde{\mathbf{b}} \dot{\tilde{\mathbf{b}}} \tag{27}$$

According to Young’s inequality, the following inequality holds:

$$m \tilde{\mathbf{b}} \dot{\tilde{\mathbf{b}}} \leq -\frac{3m \|\tilde{\mathbf{b}}\|^2}{4} + \frac{m \|\dot{\tilde{\mathbf{b}}}\|^2}{4}. \tag{28}$$

Combining (28) with (27), we obtain

$$\begin{aligned} \dot{V}_2 &\leq -k_1 \sum_{i=1}^n S_i^2 - \lambda_2 \sum_{i=1}^n h_i |S_i|^{1+\gamma} - \frac{m \|\tilde{\mathbf{b}}\|^2}{2} \\ &\quad - \frac{m \|\tilde{\mathbf{b}}\|^2}{4} + \frac{m \|\dot{\tilde{\mathbf{b}}}\|^2}{4} \\ &= -k_1 \sum_{i=1}^n S_i^2 - \lambda_2 \sum_{i=1}^n h_i |S_i|^{1+\gamma} - \frac{m \|\tilde{\mathbf{b}}\|^2}{2} + \\ &\quad \left(\frac{m \|\tilde{\mathbf{b}}\|^2}{2}\right)^{\frac{1+\gamma}{2}} - \left(\frac{m \|\tilde{\mathbf{b}}\|^2}{2}\right)^{\frac{1-\gamma}{2}} - \frac{m \|\tilde{\mathbf{b}}\|^2}{4} \\ &\quad + \frac{m \|\dot{\tilde{\mathbf{b}}}\|^2}{4}. \end{aligned} \tag{29}$$

Let  $\phi = 1, \varphi = \frac{m\|\tilde{\mathbf{b}}\|^2}{2}, p = 1 - \tilde{\gamma}, q = \tilde{\gamma}, \omega = 1$  and  $\tilde{\gamma} = \frac{1+\gamma}{2}$ . By Lemma 2, we obtain

$$\left(\frac{m\|\tilde{\mathbf{b}}\|^2}{2}\right)^{\tilde{\gamma}} \leq \Theta(\tilde{\gamma}) + \frac{m\|\tilde{\mathbf{b}}\|^2}{2}, \tag{30}$$

where  $\Theta(\tilde{\gamma}) = 1 - \tilde{\gamma}$ .

Substituting (30) into (29) leads to

$$\begin{aligned} \dot{V}_2 \leq & -k_1 \sum_{i=1}^n S_i^2 - \lambda_2 \sum_{i=1}^n h_i |S_i|^{1+\gamma} - \frac{m\|\tilde{\mathbf{b}}\|^2}{4} + \\ & - \left(\frac{m\|\tilde{\mathbf{b}}\|^2}{2}\right)^{\tilde{\gamma}} + \frac{m\|\tilde{\mathbf{b}}\|^2}{4} + \Theta(\tilde{\gamma}). \end{aligned} \tag{31}$$

By Lemma 3, it follows from (31) that

$$\dot{V}_2 \leq -\mu_1 V - \mu_2 V^{\tilde{\gamma}} + \delta \tag{32}$$

where  $\delta = \frac{m\|\tilde{\mathbf{b}}\|^2}{4} + \Theta(\tilde{\gamma}), \mu_1 = \min\{k_1, \frac{m\eta}{2}\}, \mu_2 = \min\{2^{\tilde{\gamma}}\lambda_2 h_i, (m\eta)^{\tilde{\gamma}}\}$ .

Then, by Lemma 1, the system (6) is finite-time stable with the convergence region

$$\begin{aligned} \Delta = \{ \lim_{t \rightarrow T_r} \mathbf{S} \mid V_2 \leq \min\{ & \left(\frac{\delta}{(1-\kappa)\mu_1}\right), \\ & \left(\frac{\delta}{(1-\kappa)\mu_2}\right)^{\frac{1}{\tilde{\gamma}}}\} \}, \end{aligned} \tag{33}$$

where  $0 < \kappa < 1$ ,

$$\begin{aligned} T_r \leq \max\{ & t_0 + \frac{1}{\kappa\mu_1(1-\tilde{\gamma})} \ln \frac{\kappa\mu_1 V_2^{1-\tilde{\gamma}}(t_0) + \mu_2}{\mu_2}, \\ & t_0 + \frac{1}{\mu_1(1-\tilde{\gamma})} \ln \frac{\kappa\mu_1 V_2^{1-\tilde{\gamma}}(t_0) + \kappa\mu_2}{\kappa\mu_2} \}. \end{aligned} \tag{34}$$

When  $S_i$  converges to the region  $|S_i| \leq \Delta, i = 1, \dots, n$ , it follows from (11) that

$$\begin{aligned} S_i = & e_{1i} + \frac{k_2 a}{2a-1} \cdot \text{sig}^{2-\frac{1}{a}}(e_{2i} + k_1 e_{1i}) \\ = & \vartheta_i, |\vartheta_i| < \Delta, \end{aligned} \tag{35}$$

which means both

$$\dot{e}_{1i} + e_{1i} \left(k_1 - \frac{\vartheta_i}{e_{1i}}\right) + \bar{k}_2 \text{sig}^{\bar{a}} e_{1i} = 0 \tag{36}$$

and

$$\dot{e}_{1i} + k_1 e_{1i} + \text{sig}^{\bar{a}_1} e_{1i} \left(\bar{k}_2 - \frac{\vartheta_i}{\text{sig}^{\bar{a}} e_{1i}}\right) = 0 \tag{37}$$

hold.

From (36), we can see that  $e_{1i}$  converges if  $k_1 - \frac{\vartheta_i}{e_{1i}} > 0$ . From (37), we can see that  $e_{1i}$  converges if  $\bar{k}_2 - \frac{\vartheta_i}{\text{sig}^{\bar{a}} e_{1i}} > 0$ . Hence,  $e_{1i}$  will converge to the region

$$|e_{1i}| \leq \min\left\{ \frac{\Delta}{k_1}, \left(\frac{\Delta}{\bar{k}_2}\right)^{\frac{1}{\bar{a}}} \right\} \tag{38}$$

within the finite time  $T_1 + T_r$ .  $\square$

**Remark 3.** In order to avoid the chattering phenomenon, (22) may be modified by replacing the signum function with a hyperbolic tangent function as follows:

$$\tau = -M_0 \left[ \mathbf{F}^* + \lambda_1 \mathbf{S} + \lambda_2 \text{sig}^\gamma \mathbf{S} + \hat{\mathbf{b}}^T \Phi \tanh(\mathbf{S}^T h) \right] \tag{39}$$

where  $\tanh(\mathbf{S}^T h) = [\tanh(S_1 h_1), \dots, \tanh(S_n h_n)]^T$ .

**Remark 4.** Based on Assumption 1, the robust adaptive approach is used to deal with uncertainties in this work. Additionally, these uncertainties may be approximated by adaptive neural networks and adaptive fuzzy systems [21].

**4. Simulation**

Consider a two-joint rigid robot manipulator [17] shown in Figure 2.

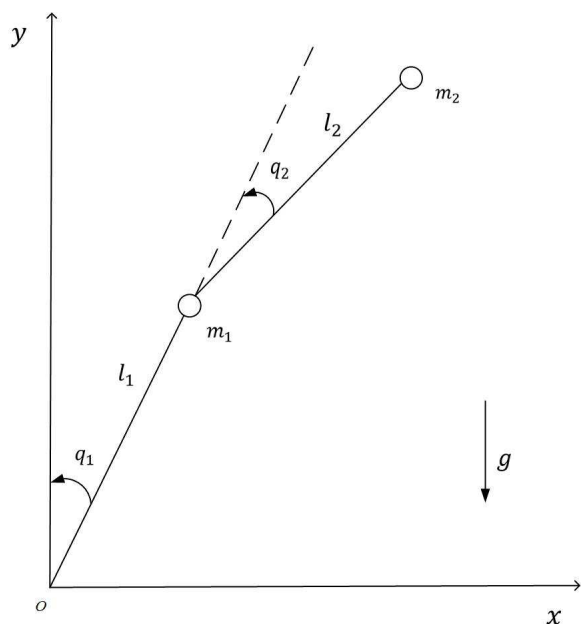


**Figure 2.** Configuration of a two-link robot manipulator.

The dynamic of robot manipulator in (1) and (2) by Lagrangian equation is represented as

$$\begin{aligned} M(q) &= \begin{bmatrix} m_{11} & m_{12} \\ m_{21} & m_{22} \end{bmatrix}, C(q, \dot{q}) = \begin{bmatrix} c_{11} & c_{12} \\ c_{21} & c_{22} \end{bmatrix}, \\ G(q) &= [g_1, g_2], \end{aligned} \tag{40}$$

where  $q = [q_1, q_2]^T$ ,  $m_{11} = (m_1 + m_2)l_1^2 + m_2l_2^2 + 2m_2l_1l_2 \cos(q_2) + J_1$ ,  $m_{12} = m_2l_2^2 + m_2l_1l_2 \cos(q_2)$ ,  $m_{21} = m_2l_2^2 + m_2l_1l_2 \cos(q_2)$ ,  $m_{22} = m_2l_2^2 + J_2$ ,  $c_{11} = -m_2l_1l_2 \sin(q_2)\dot{q}_2$ ,  $c_{12} = -m_2l_1l_2 \sin(q_2)(\dot{q}_1 + \dot{q}_2)$ ,  $c_{21} = m_2l_1l_2 \sin(q_2)\dot{q}_1$ ,  $c_{22} = 0$ ,  $g_1 = (m_1 + m_2)l_1g \cos(q_1) + m_2l_2g \cos(q_1 + q_2)$  and  $g_2 = m_2l_2g \cos(q_1 + q_2)$ . Table 1 shows the physical attributes of the manipulator used for the simulation analysis.

The reference position trajectories are  $q_{1d} = 1.25 - 1.4e^{-t} + 0.35e^{-4t}$  rad and  $q_{2d} = 1.25 + e^{-t} - 0.25e^{-4t}$  rad.  $d_1(t) = 2 \sin(t) + 0.5 \sin(200\pi t)$  N · m,  $d_2(t) = \cos(2t) + 0.5 \sin(200\pi t)$  N · m. The initial states of the robot manipulator are set as follows:  $q_1(0) = 1$  rad,  $q_2(0) = 0.5$  rad,  $\dot{q}_1(0) = 0$  rad and  $\dot{q}_2(0) = 0$  rad/s.

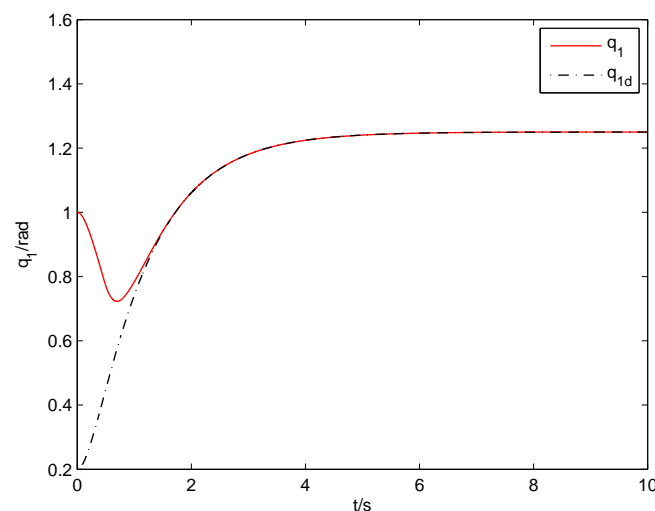
**Table 1.** Physical parameters of the two-link robot manipulator.

| Symbol   | Definition                  | Value                |
|----------|-----------------------------|----------------------|
| $l_1$    | Length of link 1            | 1.0 m                |
| $l_2$    | Length of link 2            | 0.8 m                |
| $m_{10}$ | Nominal mass of joint 1     | 0.4 kg               |
| $m_{20}$ | Nominal mass of joint 2     | 1.2 kg               |
| $m_1$    | Mass of joint 1             | 0.5 kg               |
| $m_2$    | Mass of joint 2             | 1.5 kg               |
| $J_1$    | Moment of inertia of link 1 | 5 kg.m <sup>2</sup>  |
| $J_2$    | Moment of inertia of link 2 | 5 kg.m <sup>2</sup>  |
| $g$      | Gravitational constant      | 9.8 m/s <sup>2</sup> |

The ANSFTSMC approach proposed in this paper (including nonsingular fast terminal sliding surface (11), control law (22) and adaptive law (23)) is applied for simulation, where the parameters are set as  $k_1 = 2.5, k_2 = 2, a = \frac{5}{3}, \lambda_1 = 1, \lambda_2 = 1, \gamma = \frac{3}{5}, \eta = 0.1, m = 0.001$ . The angular positions of joints 1 and 2 in are illustrated in Figures 3 and 4, respectively. The angular position error signals and angular velocity error signals of two joints are shown in Figures 5 and 6, respectively. It is observed from Figures 3–6 that favorable trajectory tracking responses are obtained by using the proposed control law. Figure 7 exhibits the control torques, which shows that the input signals are continuous and chattering-free. Figure 8 displays the parameter estimation. We can see that  $\hat{b}_1, \hat{b}_2$  and  $\hat{b}_3$  can converge to corresponding constants over time, respectively, which indicates good compensation for the uncertainties in robot manipulators.

**Remark 5.** In Section 3, the design parameters are theoretically required to meet  $k_1 > 0, k_2 > 0, a > 1, \lambda_1 > 0, \lambda_2 > 0, 0 < \gamma < 1, \eta > 0, m > 0$ . In the practical application, we recommend to set their values as follows:  $0.5 \leq k_1 \leq 5, 0.5 \leq k_2 \leq 5, 1.1 \leq a \leq 2, 0.5 \leq \lambda_1 \leq 5, 0.5 \leq \lambda_2 \leq 5, 0.1 \leq \gamma \leq 0.9, 0.02 \leq \eta \leq 0.2, 0.00005 \leq m \leq 0.1$ .

In order to verify the effectiveness of the proposed control approach, two comparisons will be carried out.

**Figure 3.** Trajectory tracking response of joint-1 (ANSFTSMC).

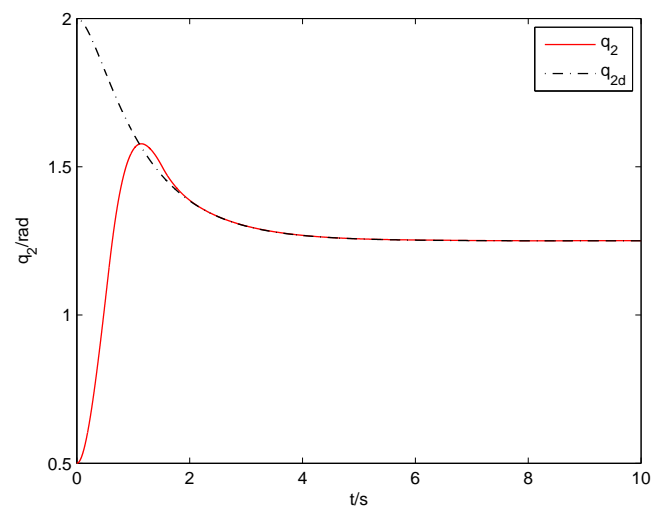


Figure 4. Trajectory tracking response of joint-2 (ANSFTSMC).

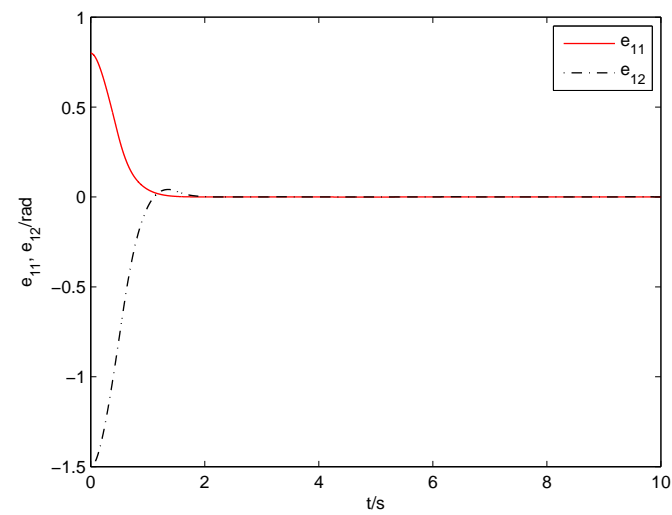


Figure 5. Position errors of joint-1 and joint-2 (ANSFTSMC).

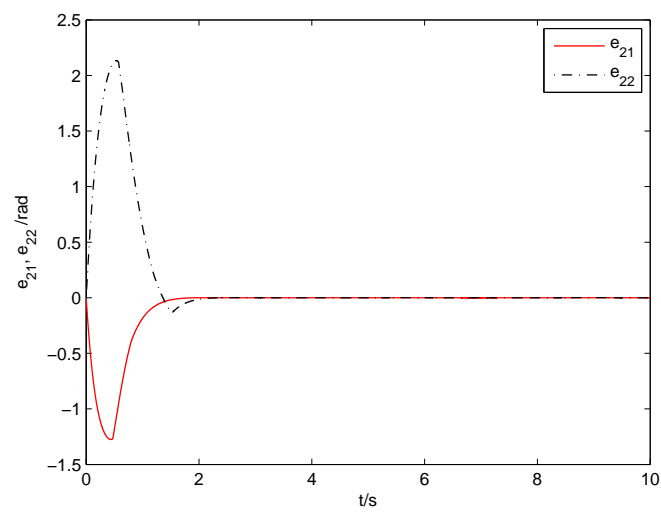


Figure 6. Velocity errors of joint-1 and joint-2 (ANSFTSMC).

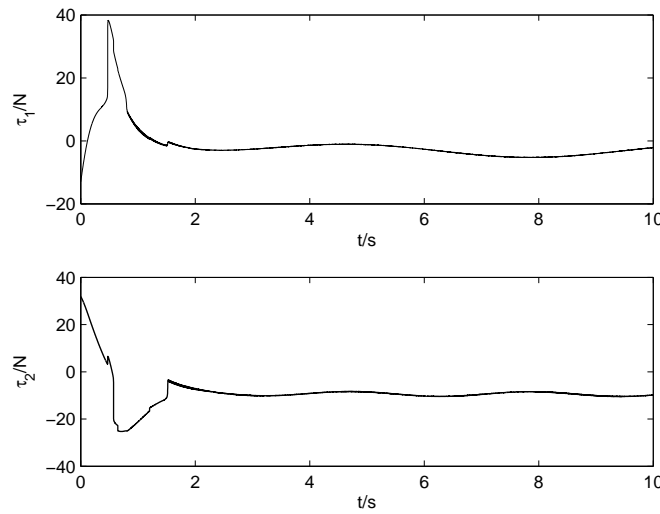


Figure 7. Control torques of joint-1 and joint-2 (ANSFTSMC).

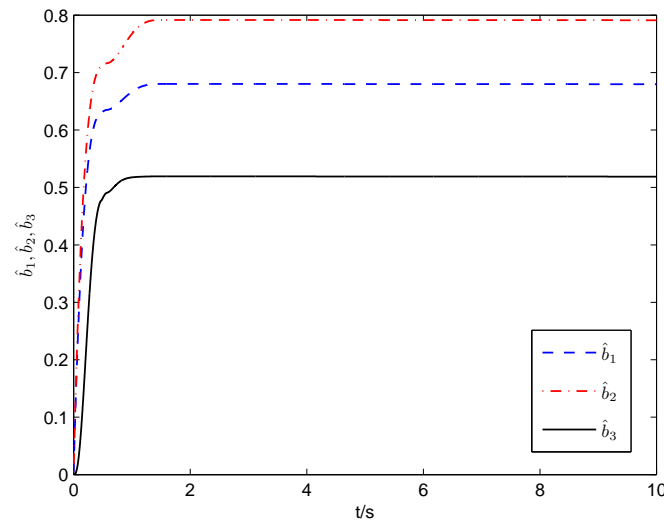


Figure 8. Parameter estimation (ANSFTSMC).

**Comparison A:** The following sliding surface and the nonsingular terminal SMC (NSTSMC) law proposed in [14] are introduced for comparison as follows:

$$\begin{aligned} S_L &= e_1 + C_1 \dot{e}_1^{\mu_2/\mu_1} \\ \tau &= \tau_0 + u_0 + u_1, \end{aligned} \tag{41}$$

where

$$\begin{aligned} \tau_0 &= C_0(q, \dot{q})\dot{q} + g_0(q) + M_0(q)\ddot{q}_d, \\ u_0 &= -\frac{\mu_1}{\mu_2} M_0(q) C_1^{-1} 2^{-\mu_2/\mu_1}, \\ u_1 &= -\frac{\mu_1 [s_L^T C_1 \text{diag}(e_1^{\mu_2/\mu_1-1}) M_0^{-1}(q)]^T}{\mu_2 \|s_L^T C_1 \text{diag}(e_1^{\mu_2/\mu_1-1}) M_0^{-1}(q)\|}. \end{aligned} \tag{42}$$

The design parameters of (41) and (42) are chosen as  $C_1 = \text{diag}[2.5, 2.5]$ ,  $\mu_1 = 3$  and  $\mu_2 = 5$ , respectively. The simulation results are shown in Figures 9–12. From them, we can see that the convergence speed of the proposed ANSFTSMC approach is faster than that of the NSTSMC algorithm.

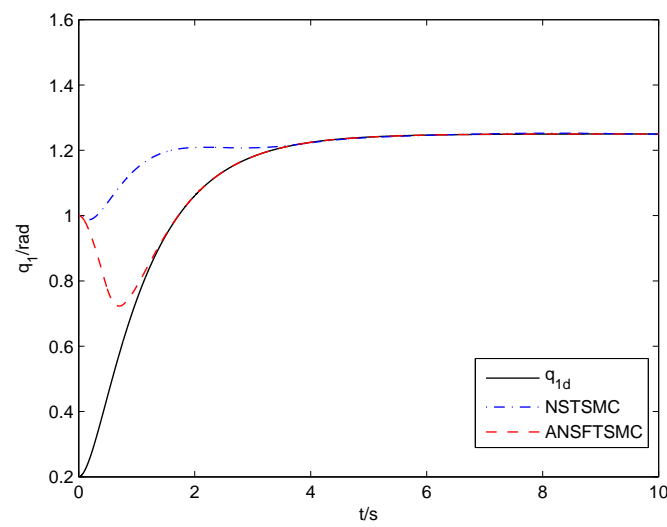


Figure 9. Trajectory tracking response of joint-1 (NSTSMC, ANSFTSMC).

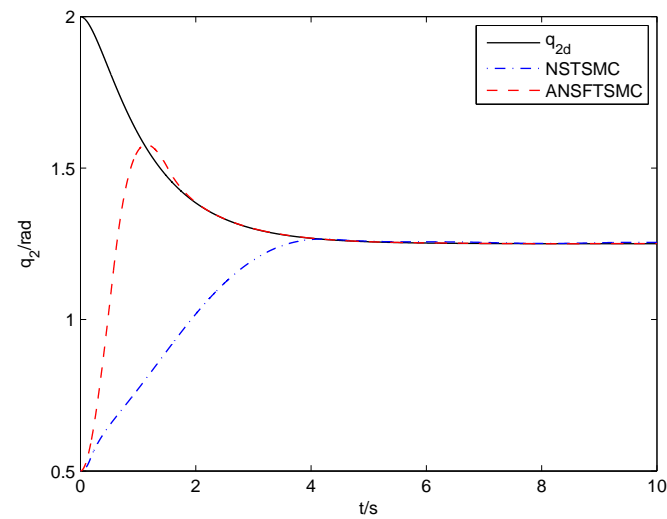


Figure 10. Trajectory tracking response of joint-2 (NSTSMC, ANSFTSMC).

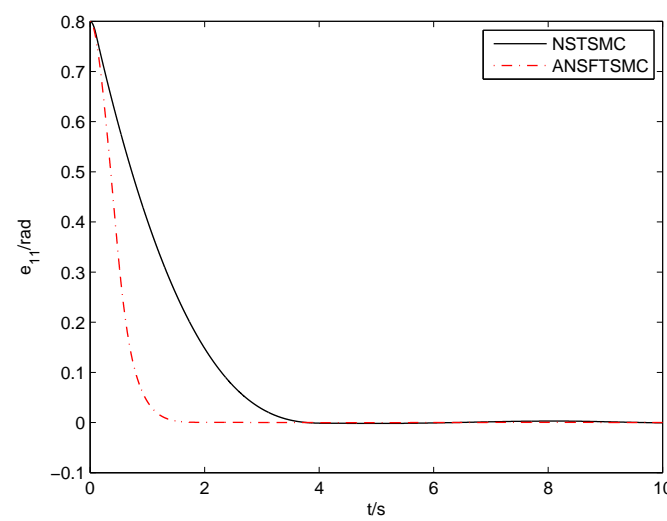


Figure 11. Position error of joint-1 (NSTSMC, ANSFTSMC).

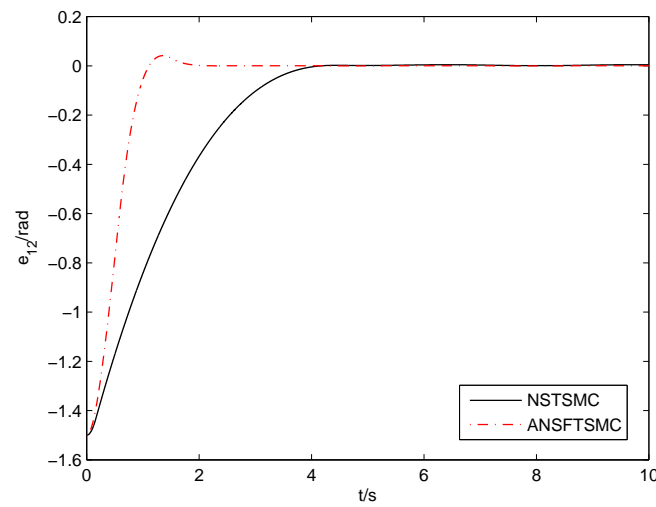


Figure 12. Position error of joint-2 (NSTSMC, ANSFTSMC).

**Comparison B:** The following sliding surface and nonsingular fast terminal SMC (NSFTSMC) algorithm are designed in light of the literature [22] as

$$\begin{aligned}
 \mathbf{S}_\Sigma &= \mathbf{e}_1 + \text{sign}^{\Gamma_1}(\mathbf{e}_1) + \text{sign}^{\Gamma_2}(\mathbf{e}_2), \\
 \boldsymbol{\tau} &= -M_0 [\zeta_2 \mathbf{S}_\Sigma + (\rho + \zeta_1) \frac{\mathbf{S}_\Sigma}{\|\mathbf{S}_\Sigma\| + \delta} + \mathbf{F} + \Gamma_2^{-1} (I_2 + \\
 &\quad \Gamma_1 \text{diag}(|\mathbf{e}_1|^{\Gamma_1 - I_2})) \text{sign}^{2I_2 - \Gamma_2}(\mathbf{e}_2)], \tag{43}
 \end{aligned}$$

where  $\zeta_1 = 1, \zeta_2 = 2, \delta = 0.01, \mathbf{S}_\Sigma = \mathbf{e}_1 + \text{sign}^{\Gamma_1}(\mathbf{e}_1) + \text{sign}^{\Gamma_2}(\mathbf{e}_2), \mathbf{F} = -M_0^{-1}(\mathbf{q})(C_0(\mathbf{q}, \dot{\mathbf{q}})\dot{\mathbf{q}} + \mathbf{G}_0(\mathbf{q})) - \ddot{\mathbf{q}}_d$ ,

$$\rho = \|M_0^{-1}\|(b_0 + b_1\|\mathbf{q}\| + b_2\|\dot{\mathbf{q}}\|), \tag{44}$$

$$b_0 = 2, b_1 = 0.5, b_2 = 0.3,$$

$$\Gamma_1 = \begin{bmatrix} 2 & 0 \\ 0 & 2 \end{bmatrix}, \Gamma_2 = \begin{bmatrix} \frac{5}{3} & 0 \\ 0 & \frac{5}{3} \end{bmatrix}, I_2 = \begin{bmatrix} 1 & 0 \\ 0 & 1 \end{bmatrix}. \tag{45}$$

As shown in Figures 13 and 14, the system angular position states track the desired reference signals quickly in the cases of NSFTSMC and ANSFTSMC, respectively. However, the ANSFTSMC system is better than NSFTSMC in convergence speed and stable precision, which can also be verified by Figures 15 and 16. In the controller design of NSFTSMC,  $b_0, b_1$  and  $b_2$  are assumed to be known (see (44)), which is required in the controller design of ANSFTSMC. Note that if the design parameter  $\delta$  is set close to zero, then the chattering phenomenon will happen. Figures 17 and 18 show the control input for the case of  $\delta = 0.01$  and  $\delta = 0$ , respectively.

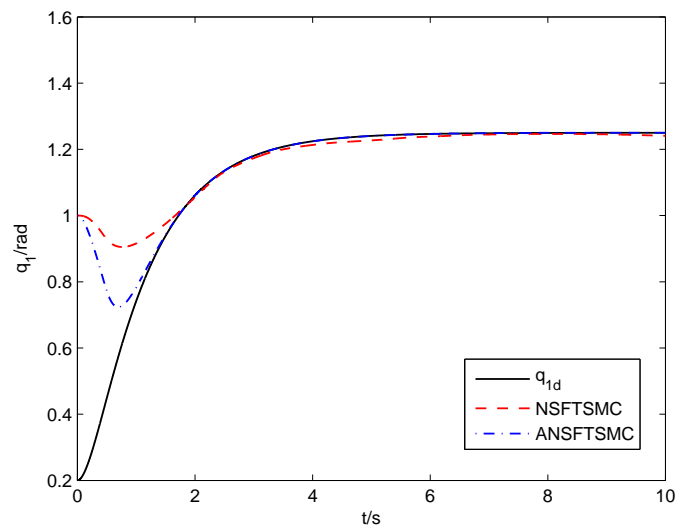


Figure 13. Trajectory tracking response of joint-1 (NSFTSMC, ANSFTSMC).

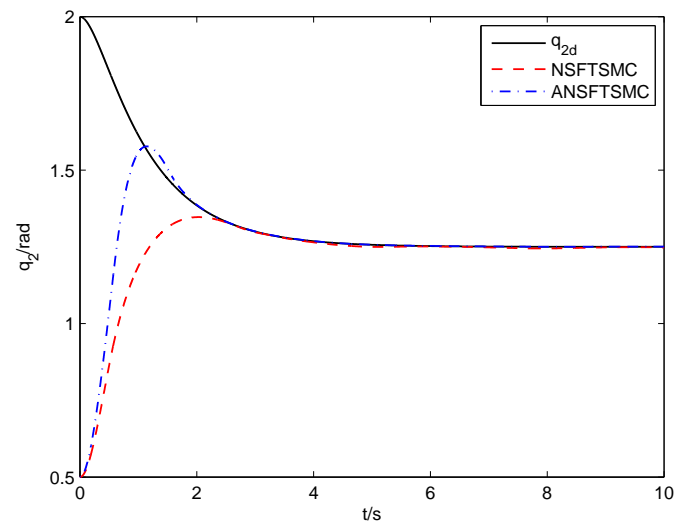


Figure 14. Trajectory tracking response of joint-2 (NSFTSMC, ANSFTSMC).

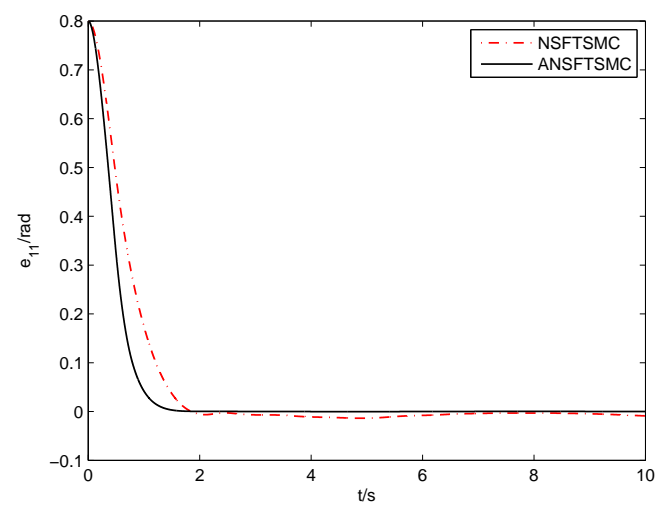


Figure 15. Position error of joint-1 (NSFTSMC, ANSFTSMC).

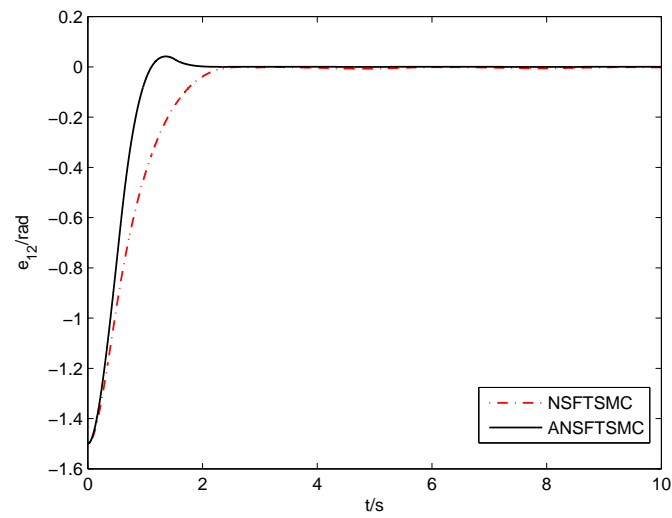


Figure 16. Position error of joint-2 (NSFTSMC, ANSFTSMC).

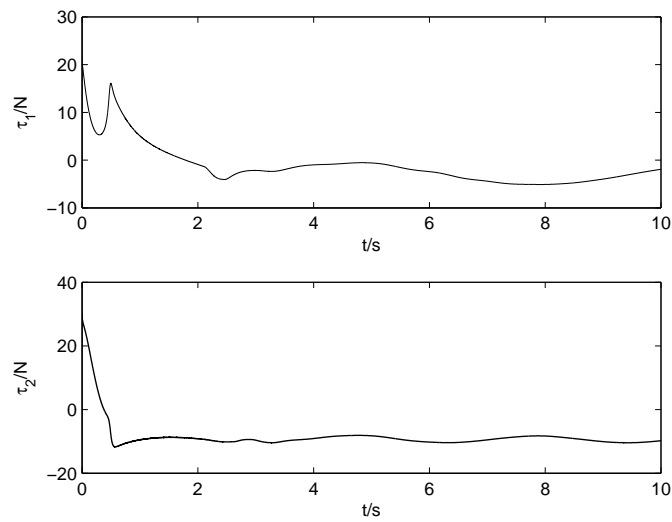


Figure 17. Control torques of joint-1 and joint-2 (NSFTSMC,  $\delta = 0.01$ ).

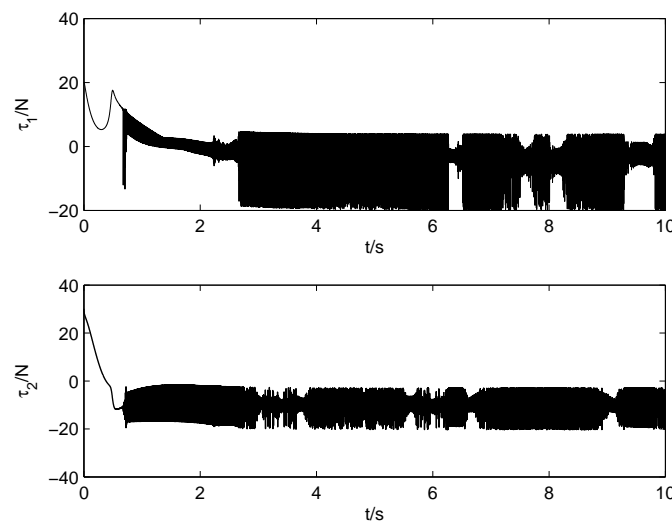


Figure 18. Control torques of joint-1 and joint-2 (NSFTSMC,  $\delta = 0$ ).

## 5. Conclusions

In this paper, an ANSFTSMC approach is proposed for robot manipulators with internal uncertainties and external disturbances to achieve a fast and high-precision trajectory tracking. We design a novel nonsingular fast terminal sliding surface and auxiliary function to avoid the singularity problem caused by the inverse matrix operation during the controller design, where the traditional piecewise continuous function approach is replaced by the auxiliary function approach to reduce the design difficulty and the burden computation. By designing an adaptive updating law, the total uncertainties, whose upper bound are unknown, in the system are compensated for. The system tracking error can converge to the neighborhood of the origin in finite time, and all the signals of the closed-loop system are guaranteed to be bounded. In future studies, we will attempt to develop an adaptive fuzzy nonsingular terminal SMC approach for robot manipulators.

**Author Contributions:** Investigation, Q.Y. and X.M.; Methodology, Q.Y. and W.W.; Project administration, D.P. All authors have read and agreed to the published version of the manuscript.

**Funding:** This work was partially supported by the National Natural Science Foundation of China under Grant 61801431, and partially supported by National Natural Science Foundation of Zhejiang Province under Grant LY22F030011.

**Data Availability Statement:** Data are contained within the article.

**Conflicts of Interest:** The authors declare no conflict of interest.

## References

1. Liu, M. Decentralized control of robot manipulators: Nonlinear and adaptive approaches. *IEEE Trans. Autom. Control.* **1999**, *44*, 357–363.
2. Kreutz, K. On manipulator control by exact linearization. *IEEE Trans. Autom. Control.* **1989**, *34*, 763–767. [[CrossRef](#)]
3. Rocco, P. Stability of PID control for industrial robot arms. *IEEE Trans. Robot. Autom.* **1996**, *12*, 606–614. [[CrossRef](#)]
4. Tayebi, A. Adaptive iterative learning control for robot manipulators. *Automatica* **2004**, *40*, 1195–1203. [[CrossRef](#)]
5. Li, X.; Yang, R.; Liu, H.; He, S. Adaptive finite-time bounded- $H_\infty$  tracking control for a class of manipulator system. *Control. Theory Appl.* **2021**, *38*, 147–156.
6. Zhao, D.; Li, S.; Zhu, Q.; Gao, F. Robust finite-time control approach for robotic manipulators. *IET Control. Theory Appl.* **2010**, *4*, 1–15. [[CrossRef](#)]
7. He, W.; Dong, Y. Adaptive Fuzzy Neural Network Control for a Constrained Robot Using Impedance Learning. *IEEE Trans. Neural Networks Learn. Syst.* **2018**, *29*, 1174–1186. [[CrossRef](#)]
8. Zhang, R.; Chen, Q. Trajectory tracking control of robotic manipulators based on smooth second-order sliding mode. *J. Syst. Simul.* **2021**, *6*, 1315–1322.
9. Zhao, L.; Cheng, H.; Wang, T. Sliding mode control for a two-joint coupling nonlinear system based on extended state observer. *ISA Trans.* **2018**, *73*, 130–140. [[CrossRef](#)]
10. Baek, J.; Jin, M.; Han, S. A New Adaptive Sliding-Mode Control Scheme for Application to Robot Manipulators. *IEEE Trans. Ind. Electron.* **2016**, *63*, 3628–3637. [[CrossRef](#)]
11. Van, M.; Ge, S. Adaptive Fuzzy Integral Sliding Mode Control for Robust Fault Tolerant Control of Robot Manipulators with Disturbance Observer. *IEEE Trans. Fuzzy Syst.* **2021**, *29*, 1284–1296. [[CrossRef](#)]
12. Tran, D.; Ba, D.; Ahn, K. Adaptive Backstepping Sliding Mode Control for Equilibrium Position Tracking of an Electrohydraulic Elastic Manipulator. *IEEE Trans. Ind. Electron.* **2020**, *67*, 3860–3869. [[CrossRef](#)]
13. Tang, Y. Terminal sliding mode control for rigid robots. *Automatica* **1998**, *34*, 51–56. [[CrossRef](#)]
14. Feng, Y.; Yu, X.; Man, Z. Non-singular terminal sliding mode control of rigid manipulators. *Automatica* **2002**, *38*, 2159–2167. [[CrossRef](#)]
15. Yu, S.; Yu, X.; Shirinzadeh, B.; Man, Z. Continuous finite-time control for robotic manipulators with terminal sliding mode. *Automatica* **2005**, *41*, 1957–1964. [[CrossRef](#)]
16. Galicki, M. Finite-time control of robotic manipulators. *Automatica* **2015**, *51*, 49–54. [[CrossRef](#)]
17. Yi, S.; Zhai, J. Adaptive second-order fast nonsingular terminal sliding mode control for robotic manipulators. *ISA Trans.* **2019**, *90*, 41–51. [[CrossRef](#)]
18. Liu, Y.; Jing, Y.; Liu, X. Survey on finite-time control for nonlinear systems. *Control. Theory Appl.* **2020**, *37*, 1–12.
19. Wang, L.; Mendel, J. Fuzzy Basis Functions, Universal Approximation, and Orthogonal Least-Squares Learning. *IEEE Trans. Neural Netw.* **1992**, *3*, 807–814. [[CrossRef](#)]
20. Zhang, G.; Huang, C.; Wu, X.; Zhang, X. Adaptive finite time dynamic positioning control of fully-actuated ship with servo system uncertainties. *Acta Autom. Sin.* **2018**, *44*, 1907–1912.

- 
21. Mohammadzadeh, A.; Taghavifar, H. A robust fuzzy control approach for path-following control of autonomous vehicles. *Soft Comput.* **2020**, *24*, 3223–3235. [[CrossRef](#)]
  22. Yang, L.; Yang, J. Nonsingular fast terminal sliding-mode control for nonlinear dynamical systems. *Int. J. Robust Nonlinear Control.* **2011**, *21*, 1865–1879. [[CrossRef](#)]